

106732
27p

Growth of Au on Ni(110): A BFS Modelling of Surface Alloy Phases

Guillermo Bozzolo
Analex Corporation
Brook Park, Ohio

Rodrigo Ibañez-Meier
WSA, Inc.
Palo Alto, California

and

John Ferrante
Lewis Research Center
Cleveland, Ohio

September 1994



National Aeronautics and
Space Administration

(NASA-TM-106732) GROWTH OF AU ON
Ni(110): A BFS MODELLING OF SURFACE
ALLOY PHASES (NASA. Lewis Research
Center) 27 p
N95-12104
Unclas
G3/26 0023908



Growth of Au on Ni(110): a BFS modelling of surface alloy phases

Guillermo Bozzolo

Analex Corporation, 3001 Aerospace Parkway, Brook Park, OH 44142-1003

Rodrigo Ibañez-Meier

WSA Inc., Palo Alto, California 94301

John Ferrante

National Aeronautics and Space Administration, Lewis Research Center, Cleveland, Ohio 44135

Abstract

Recent experiments using scanning tunneling microscopy show evidence for the formation of surface alloys of otherwise immiscible metals. Such is the case for Au deposited in Ni(110), where experiments by Pleth Nielsen et al.¹ indicate that at low Au coverage (< 0.5 ML), Au atoms replace Ni atoms in the surface layer forming a surface alloy while the Ni atoms form islands on the surface. In this work, we present results of a theoretical modelling of this phenomenon using the recently developed BFS method for alloys. We provide results of an extensive analysis of the growth process which strongly support the conclusions drawn from the experiment: at very low coverages, there is a tendency for dimer formation on the overlayer, which later exchange positions with Ni atoms in the surface layer, thus accounting for the large number of substituted dimers. Ni islands formation as well as other alternative short range order patterns are discussed.

PACS: 61.55.Hg, 68.55.Nq, 68.35.-p

I. INTRODUCTION

Recent experiments show clear evidence for surface alloying of immiscible metals [1–6]. The atomic resolution scanning tunneling microscopy (STM) experiments of Au atoms deposited on a Ni(110) surface carried out by Pleth Nielsen et al [1,2] show that in spite of the fact that Au is completely insoluble in bulk Ni, it replaces Ni atoms on the surface plane forming a surface alloy. The experiments indicate the formation of a pattern of Au dimers in the surface plane, with the displaced Ni atoms located in chains along the closed-packed (cp) direction of Ni(110), following the fcc stacking of the substrate [1]. The concept of a surface alloy for immiscible metals was corroborated by low energy ion scattering (LEIS) experiments performed by Boerma et al. [3]. In their work, they found evidence for the existence of Au atoms occupying near substitutional sites in the top Ni layer at low Au coverages. These experiments, added to the evidence advanced by the STM results and the effective medium theory calculations verifying the conditions for surface alloy formation [1], provide enough motivation to perform larger scale simulations in order to investigate this novel growth mode.

In this work, we address two fundamental issues related to this phenomenon: 1) to explore the equivalent to the ‘ordered structures’ for the case of surface alloys, that is, the mixing patterns expected to form on the surface plane, and 2) to examine the energetics of the surface alloying process of immiscible metals is a general phenomenon with the goal of establishing a criterion for the development of such type of growth. This would allow us to understand the features that distinguish the Au-Ni case from other A-B mixtures that do not form surface or bulk alloys under any conditions.

For this study we use the BFS method for alloys [7], a semiempirical technique which has had considerable success in previous applications to alloy surface phenomena. In Section II we present a brief description of the BFS method and in Section III we apply BFS to the problem of surface alloying of Au-Ni. We summarize our results in Section IV.

II. THE BFS METHOD

The BFS method is based on the idea that the energy of formation of an arbitrary alloy structure is the superposition of individual contributions ε_i of nonequivalent atoms in the alloy [7],

$$\varepsilon_i = \varepsilon_i^S + g_i(\varepsilon_i^C - \varepsilon_i^{C_0}). \quad (1)$$

so that the total energy of formation is

$$\Delta H = \sum_i \varepsilon_i \quad (2)$$

For each atom, we break up the energy into two parts: a strain energy e^S and a chemical contribution $e^C - e^{C_0}$, linked by a coupling factor g :

$$e_i = e_i^S + g_i(e_i^C - e_{0,i}^C) \quad (3)$$

where i denotes the atomic species of a given atom (e_0^C is a reference energy to be defined later).

The strain energy, e_i^S , accounts for the actual geometrical distribution of the atoms surrounding atom i , computed as if all its neighbors were of the *same* atomic species as atom i . e_i^S is then evaluated with any available technique.

The coupling term, g_i , is related to the strain energy in the sense that it contains information on the structural defect included in e_i^S . In order to establish this connection, based on the assumption that the universal binding energy relationship of Rose et al. [8] contains all the relevant information concerning a given single-component system, we write

$$e_i^S = E_C^i F^*(a_i^{S*}) \quad (4)$$

where

$$F^*(a^*) = 1 - (1 + a^*)e^{-a^*}, \quad (5)$$

and where a_i^{S*} , given by

$$a_i^{S*} = q \frac{(a_i^S - a_e^i)}{l_i}, \quad (6)$$

is a scaled lattice parameter related to a_i^S , a quantity that contains the structural information of the defect crystal. a_e^i , l_i and E_C^i , are the equilibrium lattice parameter, scaling length and cohesive energy of a pure crystal of species i and $q^3 = \frac{3}{16\pi}$ for fcc metals.

Once e_i^S is evaluated by any theoretical means, a_i^{S*} can be easily obtained from Eq.(4) with which the coupling term g_i becomes

$$g_i = e^{-a_i^{S*}}. \quad (7)$$

As in previous efforts [7], we choose equivalent crystal theory (ECT) [9] to perform strain energy calculations, the choice being guided by the simplicity and reliability of this technique. Using ECT for computing e_i^S introduces the added advantage that a_i^S (and thus a_i^{S*}) is directly obtained by solving the ECT equation for the defect crystal, as shown below. Within the framework of ECT [9], a_i^S is interpreted as the lattice parameter of an ideal, perfect crystal (i.e., the equivalent crystal) where the energy per atom is the same as the energy of atom i in the actual, defect crystal.

In general, the ECT equation for computing the strain energy reads

$$NR_1^p e^{-\alpha R_1} + MR_2^p e^{-(\alpha + \frac{1}{\lambda})R_2} = \sum_j r_j^p e^{-(\alpha + S(r_j))r_j} \quad (8)$$

(see Ref. [9] for details) where the quantities p , α , λ and the screening function S are defined in Ref. [9]. The sum on the r.h.s. of Eq. (8) runs over all neighbors of atom i at a distance r_j . Eq. (8) is then solved for the lattice parameter of the equivalent crystal a_i^S . R_1 and R_2 are the corresponding nearest- and next-nearest-neighbor distances in the equivalent crystal. The strain energy is then computed with Eq.(4). For the particular case where all the neighboring atoms are located at lattice sites, $r_j = r_1$ and $S(r_1) = 0$ for nearest-neighbors, $r_j = r_2$ and $S(r_2) = 1/\lambda$ for next-nearest-neighbors and, if n is the actual number of nearest-neighbors and m is the corresponding number of next-nearest-neighbors, then eq. (8) is simply

$$NR_1^p e^{-\alpha R_1} + MR_2^p e^{-(\alpha + \frac{1}{\lambda})R_2} = nr_1^p e^{-\alpha r_1} + mr_2^p e^{-(\alpha + \frac{1}{\lambda})r_2}. \quad (9)$$

Rigourously, the computation of the strain energy includes four terms (see Ref. [9]). In this work, we neglect the three- and four-body terms dealing with the bond angle and face-diagonal anisotropies and retain only the two-body term that accounts for bond-length anisotropies [9], which we expect to be relevant for atoms in the top (surface) layers. The higher order terms would be proportional to the small local fluctuations of the atomic positions around the equilibrium lattice sites. We expect that the leading term, Eq. (4), will properly account for these small distortions.

The chemical contribution e_i^C is obtained by an ECT-like calculation. As opposed to the strain energy term, the surrounding atoms *retain their chemical identity*, but are forced to be in equilibrium lattice sites. If N_{ik} (M_{ik}) denotes the number of nearest(next)-neighbors of species k of the atom in question (of species i) then the ECT equation [9] to be solved for the equivalent lattice parameter a_i^C is

$$NR_1^{p_i} e^{-\alpha_i R_1} + MR_2^{p_i} e^{-(\alpha_i + \frac{1}{\lambda_i})R_2} = \sum_k N_{ik} r_1^{p_i} e^{-\alpha_{ik} r_1} + \sum_k M_{ik} r_2^{p_i} e^{-(\alpha_{ik} + \frac{1}{\lambda_i})r_2} \quad (10)$$

where $N(M)$ is the number of nearest(next)-neighbors in the equivalent crystal of species i and $R_1(R_2)$ is the nearest(next)-neighbor distance in the equivalent crystal of lattice parameter a_i^C . r_1 and r_2 , are the equilibrium nearest- and next-nearest-neighbor distances in an equilibrium crystal of species i , respectively. The chemical energy is then computed with

$$e_i^C = \gamma E_C^i F^*(a_i^{C*}) \quad (11)$$

and

$$e_{0_i}^C = \gamma_0 E_C^i F^*(a_{0_i}^{C*}) \quad (12)$$

where $\gamma(\gamma_0) = +1$ if $a_i^{C*}(a_{0_i}^{C*}) \geq 0$ and $\gamma(\gamma_0) = -1$ otherwise, and $a_i^{C*} = q(a_i^C - a_e^i)/l_i$. The scaled lattice parameter a_i^{C*} is obtained from Eq.(10) with the parameters α_{ik} listed in Ref. [7], and $a_{0_i}^{C*}$ is computed by solving Eq.(10) but with $\alpha_{ik} = \alpha_i$. The rest of the parameters appearing in Eq.(10) are listed in Ref. [9].

Even though BFS is a semiempirical method, its dependence on experimental input is minimal in that *only* two experimental (or theoretical) alloy values (in the present study the heats of solution in the dilute limit were used [10]) are needed. The remaining input are pure element properties, the cohesive energy, equilibrium bulk modulus and lattice parameters. In this work, we used the parameters Δ_{AB} and Δ_{BA} determined following the procedure outlined in Ref. [7]. The experimental input, as well as the resulting BFS parameters can also be found in Ref. [7]. The BFS and ECT parameters used in this work are listed in Table 1.

III. RESULTS AND DISCUSSION

In this first BFS study of surface alloying, we will concentrate in the low-coverage regime, where the alloying effect is more pronounced [1]. Two approximations were made: while the STM experiments were carried out at room temperature [1], our simulation was done at zero temperature, in the belief that the essential ingredients that drive the alloying process will be present at zero temperature. Also, for the sake of simplicity, we ignored lattice relaxations due to either the surface or the presence of adatoms with large lattice mismatch with the substrate. This simplification allows for the study of large numbers of possible configurations without much computational effort. Moreover, previous effective medium theory calculations [1] indicate that both approximations are reasonable in the sense that evidence for surface alloying is found even if relaxation and temperature effects are left out of the simulation.

There are at least two ways of performing this simulation: a systematic one, where Monte Carlo techniques can be used to determine the equilibrium configuration for a certain coverage, or a ‘brute-force’ one, where specific configurations are chosen to study the detailed processes taking place and the behavior of individual atoms. We chose the latter: by examining a sufficiently large number of possible configurations, even those that are energetically unfavorable, we expect to gain some insight that could later be applied for similar systems and therefore search for a general criterion.

The calculation was performed on a Ni slab several layers deep, with a (110) surface. Varying numbers of Au atoms were deposited and located in substitutional sites in the top or inner layers, or just as adatoms on hollow sites of the Ni(110) surface.

We will analyze the results in terms of the energy of formation of a given configuration, and the contributions of individual atoms, as defined in eq.(3), to that magnitude. Let δH be the energy of formation per impurity atom (in eV/atom):

$$\delta H = \frac{\Delta H - \Delta H_0}{N_{Au}} \quad (13)$$

where ΔH is the energy of formation of the configuration, ΔH_0 is the corresponding value for a free Ni surface and N_{Au} is the number of impurity atoms. Starting with a single Au adatom deposited on a hollow site on the Ni substrate, it is seen that it contributes so that the energy of formation of the cell considered is reduced by -0.629 eV. Within the framework of BFS, this is due to the decrease of the strain energy of the four Ni atoms on the surface plane as they increase their coordination by having the Au atom as a nearest-neighbor. Furthermore, the chemical energy contributions from these Ni atoms and the Au atom are also negative. The change in energy due to the addition of a second Au adatom depends on its location in the overlayer with respect to the first: δH is -0.629 eV if the two adatoms are far from each other, and it varies from -0.624 eV to -1.08 eV for dimers located in the (diagonal) direction and the close-packed (cp) direction, respectively. Additional adatoms have basically the same effect: clustering along the cp direction always reduces δH , with the formation of a Au chain being the preferred configuration. As we will see in detail later for $N_{Au} = 4$, it is interesting to note that two configurations involving Au dimers are very close in energy to the Au chain, always along the cp direction. This supports the claim of the likelihood of dimers being formed on the overlayer before the exchange with Ni atoms begins.

Returning to the case of just one Au atom, it is interesting to study the different configurations in terms of the strain, glue, and chemical energy, as described by eq.(3): δH results from a delicate balance between these quantities. It was noted above that while the chemical energy contribution from the Ni-Au bonds is negative, its effect in lowering δH is ‘modulated’ by the value of the glue term, g , which in turn depends on the magnitude of the strain energy contribution (see ref. [7] for a detailed description of the calculation of the different terms in eq.(3)). As the impurity atom penetrates into the Ni substrate occupying sites on the surface plane and the planes below, it reduces its strain significantly, as it finds increasing coordination as well as a much higher electron density due to the difference in size between Au and Ni atoms. Therefore, with ϵ_{Au}^S lower, the glue term increases in magnitude, emphasizing the negative contribution to δH due to the chemical energy. However, beyond

the surface plane the strain increases again as the Au atom finds itself in a compressed bulk-like environment, thus reducing the glue and the negative contribution of the chemical energy. A quick estimate illustrates this argument: the calculation of the BFS strain energy (to a nearest-neighbor approximation) is based on a ‘measure’ of the defect as seen by a given atom. Eq. (9) establishes a relationship between the defect crystal (r.h.s. of the equation) and the equivalent crystal (l.h.s.). The term to the left could be understood as a measure of the defect, given by (in a nearest-neighbor approximation) $q_d = nr^p e^{-\alpha r}$ [7], where n is the number of nearest-neighbors located at a distance r of the atom in question (assuming, as is the case in this unrelaxed calculation, that the separation distance between nearest-neighbors is the same in all cases). The parameters p and α depend on the species of the reference atom [7,9]. Equilibrium (a situation for which both sides of eq.(8) are identical) corresponds to $q_e = Nr_e^p e^{-\alpha r_e}$, where $N = 12$ and $r_e = \sqrt{2}a_e/2$ (for fcc metals). For a Au atom in a Ni lattice we could ask ourselves what is the effective number of Ni nearest-neighbors that will simulate the equilibrium situation for a Au atom (i.e., what is the value of n for which $q_d = q_e$):

$$nr_{Ni}^{p_{Au}} e^{-\alpha_{Au} r_{Ni}} = Nr_{Au}^{p_{Au}} e^{-\alpha_{Au} r_{Au}} \quad (14)$$

where r_X is the equilibrium nearest-neighbor distance for species X , $p_{Au} = 10$ and $\alpha_{Au} = 4.339$ [9]. It turns out that $n \sim 9.4$, which means that if the Au atom is surrounded by n Ni atoms in a Ni lattice it would have no strain energy. Conversely, a Au atom in a substitutional site in the Ni(110) surface with seven Ni nearest-neighbors at Ni equilibrium distances has the same strain energy that it would have in a Au lattice with 8.9 Au nearest-neighbors. If the number of nearest-neighbors was a continuous variable, the Au atom would be in equilibrium somewhere between the top two layers of the Ni slab.

Table 2 displays the values of δH for the Au atom located a) in the overlayer (O), b) in a substitutional site on the surface plane (S) with the substituted Ni atom in the overlayer as a nearest-neighbor, c) same, with the substituted Ni atom in the overlayer far from the impurity, d) in the first plane below the surface (1b) and e) two planes below the surface

plane (2b). The intermediate columns indicate the values of ϵ_{Au}^S , g_{Au} and $\epsilon_{Au}^C - \epsilon_{Au}^{Co}$ (δH , of course, includes the contributions from the Ni atoms).

The small difference in δH between configurations (b) and (c) can be easily explained in terms of the larger number of surface Ni atoms in (c) affected by the impurity atom and the substituted Ni atom in the overlayer: this is illustrated in Table 3, where the contribution from each layer is listed for each case. As a reference, we also indicate the corresponding contributions from a free Ni surface (i.e., no Au atoms present).

Most configurations with two impurity atoms are energetically favored with respect to those with a single Au atom: our results show that a Au dimer immersed in the surface layer, with the substituted Ni atoms forming a dimer somewhere else in the overlayer have the lowest energy (with both dimers oriented in the cp direction) with respect to the two Au atoms and two substituted Ni atoms in other locations: following the structure of Table 3, Table 4 displays the contributions from different layers for the following configurations: a) two isolated Au adatoms in the overlayer [(O)Two adatoms], b) a gold dimer in the overlayer [(O)Au₂], c) a gold dimer in the surface plane with a Ni dimer in the overlayer, nearest-neighbors [(S)Au₂, (O)Ni₂, NN], d) a gold dimer in the surface plane with a Ni dimer somewhere else in the overlayer [(S)Au₂, (O)Ni₂, far], e) a gold dimer one plane below the surface with the Ni dimer somewhere else in the overlayer [(1b)Au₂, (O)Ni₂, far] and f) a gold dimer two planes below the surface with the substituted Ni dimer in the overlayer [(2b)Au₂, (O)Ni₂]. These last two cases are included to highlight the fact that Au dimers penetrate, at the most, into the surface layer. We also list the energy of formation of the cell per impurity atom as well as the results for a free surface.

So far, we can conclude that the essential features indicated in the experiments of Pleth Nielsen et al. [1] for very low coverages are reproduced by this theoretical calculation: there is strong indication that after deposition dimers tend to form on the overlayer along the close-packed direction, and later occupy substitutional sites in the Ni substrate, but only in the surface plane. Moreover, although the configuration [(S)Au₂, (O)Ni₂, far] is preferred

for $N_{Au} = 2$. As we will see below, higher coverages alter the distribution of Ni atoms in the overlayer leading to alternative island shapes, as we will see below.

Obviously, increasing the number of deposited Au atoms leads to countless configurations, impossible to analyze in any systematic fashion. We therefore limit the following examples to those cases where every multi-atom arrangement is restricted to be oriented in the cp direction and the gold atoms are restricted to be located only in the overlayer and/or the surface plane. In a cell with 60 atoms in each plane, the case with $N_{Au} = 4$ corresponds to a coverage of 0.067 ML. Assuming periodicity, the cp chain (fig.(1.a)) has the lowest energy per impurity atom among all the possible configurations with all four Au atoms in the overlayer ($\delta H = -1.290$ eV) as compared to other configurations shown. In fig. 1, Ni atoms are indicated by small circles (surface plane) or large circles (overlayer), Au atoms are correspondingly indicated by small and large disks. Also, for reasons of space, we limit the all the figures in this work to display only the ‘active’ region of the 60 atoms cell (i.e., the region affected by the Au atoms and the substituted Ni atoms). Not surprisingly, the next possible configuration corresponds to two cp dimers, far from each other (fig. 1.b). This is followed by different island shapes, as illustrated in figs. (1.c-h). The corresponding values of δH are listed in table 5. in order of decreasing energy.

However, there are several configurations with lower energy for the same coverage: these correspond to the case when the Au atoms *substitute* Ni atoms in the surface layer, with the displaced Ni atoms forming cp chains of four atoms in the overlayer. The difference between these configurations is in the relative position of the Au atoms inserted in the surface layer: fig. 2 indicates six of the lowest energy configurations and table 6 lists the corresponding energies: all of them are lower than (a) in table 5 (the lowest energy configuration with all the Au atoms in the overlayer), indicating that arrangements that include long Ni chains surrounded by Au dimers are among the most likely configurations. From these results one can see, even at this very low coverage, clear indication of the trends which ultimately will lead to the situations found experimentally. These configurations share some distinctive features: the penetration of Au atoms in the surface layer, the formation of Ni chains in

the overlayer along the close-packed direction and the ‘linkage’ of the Au atoms and the substituted Ni atoms by means of an intermediate surface Ni atom. We illustrate these last two issues in fig. 3: the distinction between figs. 3.a and 3.b is given by the shape of the Ni island: fig. 3.a shows a 4-atom Ni chain while fig. 3.b displays the same chain but broken into two separate Ni dimers, with a substantial increase in energy as indicated in table 7.

An interesting detail is the fact that the configuration shown in fig. 3.a has a lower energy δH than the one shown in fig. 3.f, the difference between the two being the orientation of the Au dimers in the surface layer. Our previous discussion would lead us to expect the second one to be lower in energy because of the orientation of the dimer in the close-packed direction, but that is not the case. On the one hand, it is clear that the advantage for the fig. 3.a configuration is that it maximizes the gain in energy due to the particular linkage between the Au atoms and the substituted Ni atoms: by positioning themselves perpendicular to the close-packed direction, all four Au atoms benefit from the gain due to the linkage effect discussed above. On the other hand, the question arises if this is a configuration with a high probability for existence. The answer is clearly no: as proven earlier, there is a strong likelihood that the Au atoms deposited on the Ni substrate will migrate to form dimers oriented in the close-packed direction. While $\delta H = -1.0806$ eV for a Au dimer in the close-packed direction, it is just -0.6287 eV for a dimer in the perpendicular direction. Moreover, two isolated Au adatoms have an even lower energy than that ($\delta H = -0.6291$ eV). This would be followed by an exchange of Au and Ni dimers, with the substituted Ni dimers forming island on the overlayer. It was shown that, once again, dimers will conserve their orientation after the exchange process. Finally, once squeezed out from the surface layer, the Ni atoms will migrate on the substrate forming islands with close-packed chains as their basic structure. Therefore, in an experimental case, the configurations shown in figs. 3.a and 3.b are highly unlikely to be found.

The remainder of fig. 3 shows three rather similar configurations for two different Au coverages (0.033 and 0.067 ML), where the difference resides in the relative location of the Au dimers and the Ni chain: the gain in energy is maximized when they are connected by

a Ni substrate atom (boxed in fig. 3.d and 3.g). Table 7 lists the energy contributions per layer, showing the small changes taking place when evolving from fig. 3.c to 3.e ($N_{Au} = 2$) and fig. 3.f to 3.h ($N_{Au} = 4$).

As we increase the coverage, a pattern emerges: the energy spectrum of the large number of configurations available shows a tendency to group into energy ‘bands’ in the sense that within each group there are small differences in energy while the energy gap between each ‘band’ is much larger. Also, each group of configurations are characterized by a certain symmetry: in the lower end of the spectrum, we always find configurations where the essential features are Au atoms in the surface plane, forming dimers, and the substituted Ni atoms forming a chain along the cp direction in the overlayer, as shown in fig. 4. The difference among the configurations belonging to this group is given by the location of the dimers with respect to the Ni chain. These findings are consistent with the large dimer concentration seen in the STM experiments [1].

However, as the coverage increases, new configurations appear in this ‘ground state’ group: those where the Au adatoms form long chains along the cp direction in the overlayer (fig. 4.d). This could be taken as an indication of growth of the Au film on the substrate in competition with the formation of a surface alloy. A first hint of this alternative can already be seen at relatively low coverages: table 8 shows some results for 0.13 ML and 0.17 ML Au coverage, with the corresponding configurations represented in fig. 4.

A possible explanation for this change in growth pattern can be found in terms of the surface energy of Au being much lower than that of Ni: for low coverages, the decrease in energy driving the penetration of Au atoms in the surface layer is guided by the effective coordination effect mentioned earlier: Au atoms ‘benefit’ from locating themselves in the surface layer, with the Ni atoms forming islands in the overlayer. At one point, the increase in surface energy due to the large Ni islands becomes larger than any gain generated by the intermixing of Au and Ni atoms in the surface plane, therefore, configurations with Au islands on the Ni substrate become energetically favored thus reverting to a normal growth mode where Au atoms tend to form a pure Au layer. The breaking point between

these two regimes seems to be around a Au coverage of 0.5 ML. For higher coverages, there is experimental indication that alternative 3D pattern formation starts. This will be the subject of future work. To illustrate these observations, we consider a few configurations corresponding to 0.5 ML coverage. Fig. 5 shows three configurations with 30 Au atoms in a 60 atoms-per-plane cell. Fig. 5.a shows a highly disordered distributions, dominated by the presence of Au dimers inserted in the surface plane, separated by irregular Ni islands in the overlayer. All 30 Au atoms are located in the surface. Fig. 5.b shows a highly ordered distribution, where the Au atoms are sandwiched between two Ni layers. Fig. 5.c displays a large Au island on the pure Ni substrate. The corresponding numerical results are listed in table 9: the contribution of each layer (following the format in table 2) to the total energy of formation is shown, confirming our previous assumption. For completeness, we also show results for the pure Ni slab (no Au coverage) to highlight the surface effects generated by the presence of the Au atoms and their distribution. The dimer+island configuration (fig. 5.a) is characterized by Au dimers losely linked to the Ni islands: if the Au dimers where covered by substituted Ni atoms, as is the case in fig. 5.b, they would have their strain energy increased to levels where little gain is realized from the substitution process: the contribution from the surface layer jumps from 13.707 eV in fig. 5.a to 48.541 in fig. 5.b. Also, in fig. 5.b there is a large contribution from the Ni overlayer (45.403 eV) due to the high surface energy of Ni. In fig. 5.c, the reversal brings stabilization to a ‘sandwich’ distribution: the Au overlayer has a noticeable lower contribution (14.469 eV vs. 45.403 for Ni) and the surface of Ni lowers its energy substantially (47.196 eV) with respect to a free Ni surface (96.582 eV).

IV. CONCLUSIONS

Summarizing the results presented for different coverages, we can imagine the sequence of events that lead to the situation observed experimentally: The first few Au adatoms are readily adsorbed on the Ni surface with a tendency to migrate until they form dimers along the close-packed direction. These dimers are then exchanged with Ni atoms on the surface plane conserving their original orientation. The displaced Ni atoms tend to form islands along the close-packed direction trying to keep a certain level of 'linkage' with the Au dimers embedded in the surface layer. This process leads to the formation of islands whose ultimate shape is therefore determined by the relative location of the Au dimers in the surface plane. For low coverages (less than 0.5 ML) this arguments explain the experimental results observed. Two processes compete to bring a delicate balance that essentially favors the formation of a surface alloy: the energetically favorable intermixing of Au atoms in the surface plane due to the increased effective coordination perceived by those surface atoms, and the energetically unfavorable formation of islands with the substituted Ni atoms, with an increase in energy due to the lower coordination. As the size of these islands grows, more energy gain is realized by a direct deposition of a Au overlayer as opposed to the formation of a surface alloy. The final configuration is, obviously, strongly dependent on the experimental conditions, as it could also be possible that in a slow deposition process, the Ni islands could allow for the formation of additional surface alloy cells therefore generating a disordered alloy pattern that goes beyond the single-layer alloy formed at low coverages. A 'sudden' coating of Au would not allow for the formation of any surface alloy at all.

The experimental evidence available for high coverages shows the evidence of interesting growth patterns which we plan to analyze in future efforts: undoubtedly, these features are a direct consequence of the low miscibility between the two participating elements and a careful numerical study of the type presented in this work might be helpful to gain insight in this new growth process.

ACKNOWLEDGMENTS

Fruitful discussions with Dr. N. Bozzolo are gratefully acknowledged. This work was partially supported by the Engineering Directorate, NASA Lewis Research Center.

REFERENCES

- [1] L. Pleth Nielsen, F. Besenbacher, I. Stensgaard, E. Lægsgaard, C. Engdahl, P. Stoltze, K. W. Jacobsen and J. K. Nørskov, *Phys. Rev. Lett.* **71**, 754 (1993).
- [2] L. Pleth Nielsen, I. Stensgaard, E. Lægsgaard and F. Besenbacher, *Surf. Sci.* **307-309**, 544 (1994).
- [3] D. O. Boerma, G. Dorenbos, G. H. Wheatley and T. M. Buck, *Surf. Sci.* **307-309**, 674 (1994).
- [4] E. I. Altman and R. J. Colton, *Surf. Sci. Lett.* **304**, L400 (1994).
- [5] Y. -R. Tzeng, H. -T. Wu, K. -D. Shiang and T. T. Tsong, *Phys. Rev. B* **48**, 5549 (1993).
- [6] D. D. Chambliss, R. J. Wilson and S. Chiang, *J. Vac. Sci. Technol. A* **10**, 1992 (1993).
- [7] G. Bozzolo, J. Ferrante and J. R. Smith, *Phys. Rev. B* **45**, 493 (1992); G. Bozzolo and J. Ferrante, *Scr. Met. Mater.* **26**, 1275 (1992); *Phys. Rev. B* **45**, 12191 (1992); *Phys. Rev. B* **46**, 8600 (1992); *Ultramicroscopy* **42-44**, 55 (1992); G. Bozzolo, B. Good and J. Ferrante, *Surf. Sci.* **289**, 169 (1993); B. Good, G. Bozzolo and J. Ferrante, *Phys. Rev. B* **48**, 18284 (1993); R. Kobistek, G. Bozzolo, J. Ferrante and H. Schlosser, *Surf. Sci.* **307-309**, 390 (1994).
- [8] J. H. Rose, J. R. Smith and J. Ferrante, *Phys. Rev. B* **28**, 1835 (1983); J. H. Rose, J. R. Smith, F. Guinea and J. Ferrante, *Phys. Rev. B* **29**, 2963 (1984).
- [9] J. R. Smith and A. Banerjea, *Phys. Rev. Lett.* **59**, 2451 (1987); *Phys. Rev. B* **37**, 10411 (1988); J. R. Smith, T. Perry, A. Banerjea, J. Ferrante and G. Bozzolo, *Phys. Rev. B* **44**, 6444 (1991)
- [10] R. Hultgren, R. L. Orr, P. D. Anderson and K. K. Kelley, *Selected Values of the Thermodynamic Properties of Binary Alloys* (Wiley, New York, 1963).

Element	Cohesive Energy	Lattice Constant	p	l	α	λ
Au	3.78	4.078	10	0.236	4.339	0.663
Ni	4.435	3.524	6	0.270	3.015	0.759

BFS : $\Delta_{AuNi} = -0.05062$, $\Delta_{NiAu} = -0.06225$

Table 1 : Experimental input: Cohesive energy (in eV), lattice parameter (in Å). ECT parameters: p , l (in Å), α (in Å⁻¹) and λ (in Å) for several fcc elements. The last entry displays the BFS parameters Δ_{AB} and Δ_{BA}

Conf.	ϵ_{Au}^S	g_{Au}	$\epsilon_{Au}^C - \epsilon_{Au}^{C_0}$	ϵ_{Au}	δH
a: (O)	1.3670	0.2810	-0.3506	1.2683	-0.62912
b: (S)	0.2125	0.6840	-0.4574	-0.1003	-0.76245
c: (S)	0.5326	0.5186	-0.4469	0.3009	-0.79218
d: (1b)	0.6873	1.6610	-0.2449	0.2806	0.66555
e: (2b)	3.5988	2.6699	-0.9820	0.9581	1.47555

Table 2: One Au atom in different locations (see text). The strain energy, glue and chemical energy contributions are listed in the second, third and fourth column, respectively. The fifth column displays the total contribution to the energy of formation from the Au atom and the last column shows the total energy of formation per impurity atom of the cell. All energies are in eV.

Configuration (see text)	ΔH Overlayer	ΔH Surface	ΔH 1-below	ΔH 2-below	δH
(a) Free surface	0.	24.1456	1.9797	0.	
(b)	2.4516	21.1392	1.7753	-0.0032	-0.76245
(c)	2.4604	21.1204	1.7555	-0.0032	-0.79218

Table 3: Contributions per layer to the energy of formation of a free Ni surface (a), a surface with a Au atom in a substitutional site in the surface plane, with the substituted Ni atom nearby (b) and the same case when the Ni atom is somewhere else in the overlayer (c). The energies, in eV, correspond to a rectangular slab with 15 atoms per plane with a coverage of 0.04 ML.

Configuration (see text)	ΔH Overlayer	ΔH Surface	ΔH 1-below	ΔH 2-below	δH
Free surface	0	28.9747	2.37564	0	
(O)Two adatoms	2.53670	25.4532	2.10225	0	-0.62912
(O)Au ₂	1.61365	25.4718	2.10367	0	-1.08063
(S)Au ₂ , (O)Ni ₂ , NN	4.03907	23.2476	1.98288	-0.0065	-1.04367
(S)Au ₂ , (O)Ni ₂ , far	4.07538	23.0621	1.93337	-0.0065	-1.14302
(1b)Au ₂ , (O)Ni ₂	4.07538	25.5170	2.55011	-0.0400	0.37305
(2b)Au ₂ , (O)Ni ₂	4.07538	25.6121	1.95342	3.0621	1.65313

Table 4: Contribution per layer to the heat of formation of a cell with 18 atoms per plane. δH indicates the energy of formation per impurity atom for several configurations with two Au atoms (0.036 ML).

Config. (Fig. 1)	δH [eV/atom]	Config. (Fig. 1)	δH [eV/atom]
(1.a)	-1.29000	(1.e)	-1.06248
(1.b)	-1.08063	(1.f)	-1.06191
(1.c)	-1.07830	(1.g)	-1.05311
(1.d)	-1.07193	(1.h)	-1.03737

Table 5: Energy of formation per impurity atom δH for Au coverage of 0.067 ML for the configurations indicated in fig. 1.

Config. (Fig. 2)	δH [eV/atom]	Config. (Fig. 2)	δH [eV/atom]
(2.a)	-1.39647	(2.d)	-1.34286
(2.b)	-1.34872	(2.e)	-1.34122
(2.c)	-1.34664	(2.f)	-1.33580

Table 6: Energy of formation per impurity atom δH for Au coverage of 0.067 ML for the configurations indicated in fig. 2.

Configuration (see text)	ΔH Overlayer	ΔH Surface	ΔH 1-below	ΔH 2-below	δH
Fig. (3.a)	7.3006	84.5845	7.0360	-0.0131	-1.39825
Fig. (3.b)	8.1507	84.5504	7.0340	-0.0131	-1.19464
Fig. (3.c)	4.0754	90.6698	7.4765	-0.0065	-1.14302
Fig. (3.d)	4.0754	90.6656	7.4765	-0.0065	-1.14512
Fig. (3.e)	4.0633	90.6839	7.4962	-0.0065	-1.13218
Fig. (3.f)	7.3006	84.7913	7.0358	-0.0131	-1.34664
Fig. (3.g)	7.3006	84.7829	7.0359	-0.0131	-1.34872
Fig. (3.h)	7.2764	84.8195	7.0752	-0.0131	-1.33580

Table 7: Contribution per layer to the heat of formation of a cell with 60 atoms per plane. δH indicates the energy of formation per impurity atom for several configurations with a-b) four Au atoms (0.067ML), c-e) a Au and a Ni dimer (0.033 ML) and f-h) Au dimers and a Ni chain (0.067 ML).

Config. (Fig. 4)	δH [eV/atom]	Config. (Fig. 3)	δH [eV/atom]
(4.a)	-1.44847	(3.d)	-1.49735
(4.b)	-1.39317	(3.e)	-1.39389
(4.c)	-1.33580	(3.f)	-1.37870

Table 8: Energy of formation per impurity atom δH for Au coverage of 0.13 ML (left columns) and 0.17 ML (right columns) for the configurations indicated in fig. 4.

Configuration (see text)	ΔH Overlayer	ΔH Surface	ΔH 1-below	ΔH 2-below	δH
Free surface	0.	96.5824	7.9188	0.	
Fig. (5.a)	54.6839	13.7072	2.0384	-0.0983	-1.13900
Fig. (5.b)	45.4026	48.5411	3.6298	0.0449	-0.22943
Fig. (5.c)	14.4691	47.1964	5.0121	0.1304	-1.25644

Table 9: Contributions per layer to the energy of formation of a free Ni surface, and each of the three configurations shown in fig. 5. The energies are in eV (ΔH) and eV/atom (δH) and correspond to a rectangular slab with 60 atoms per plane with a Au coverage of 0.50 ML.

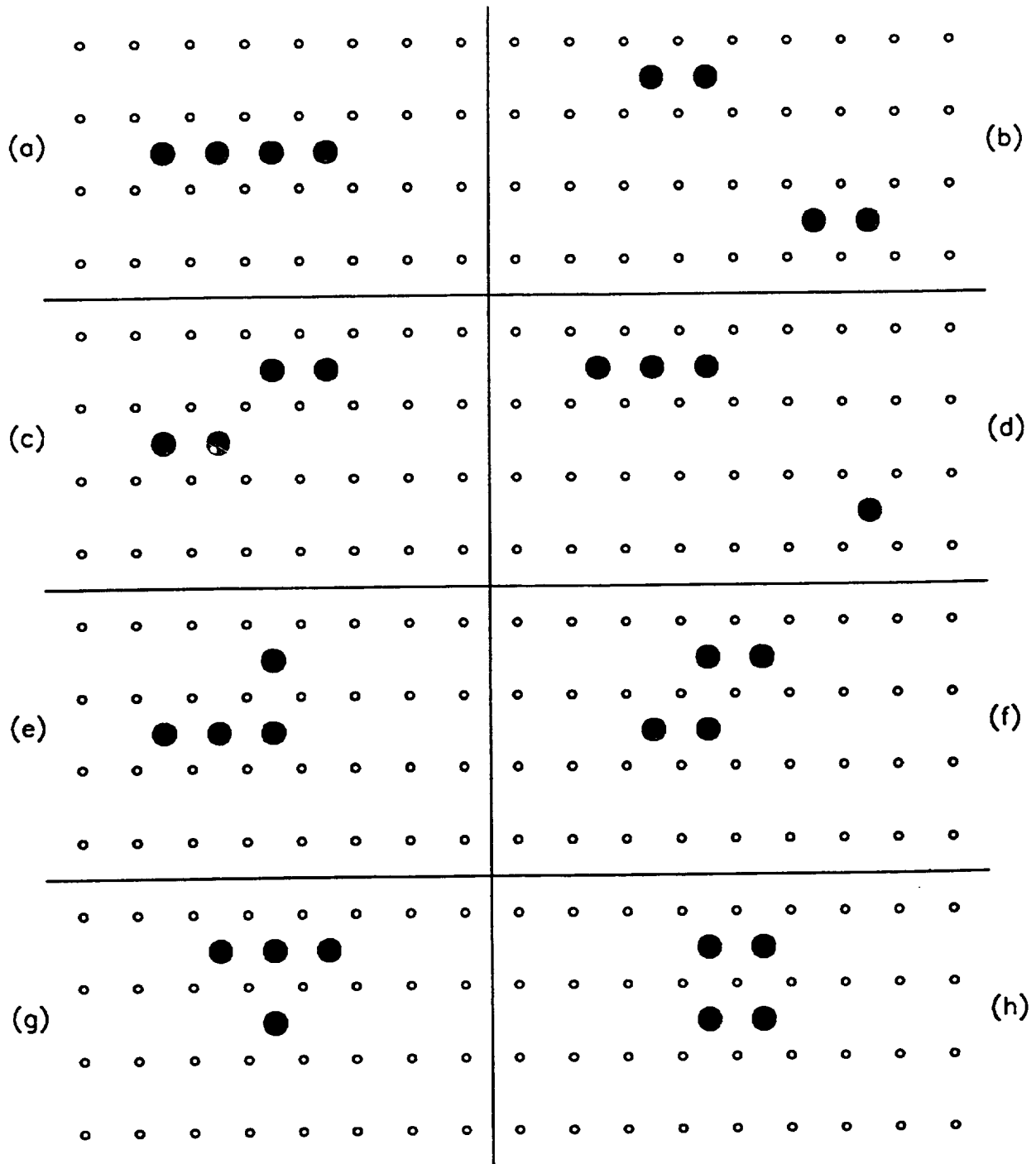


Fig. 1 : Schematic representation of the Ni(110) surface: small circles (o) indicate Ni atoms in the surface layer; Au atoms in the overlayer are indicated by large disks (●). These configurations correspond to a Au coverage of 0.067 ML.

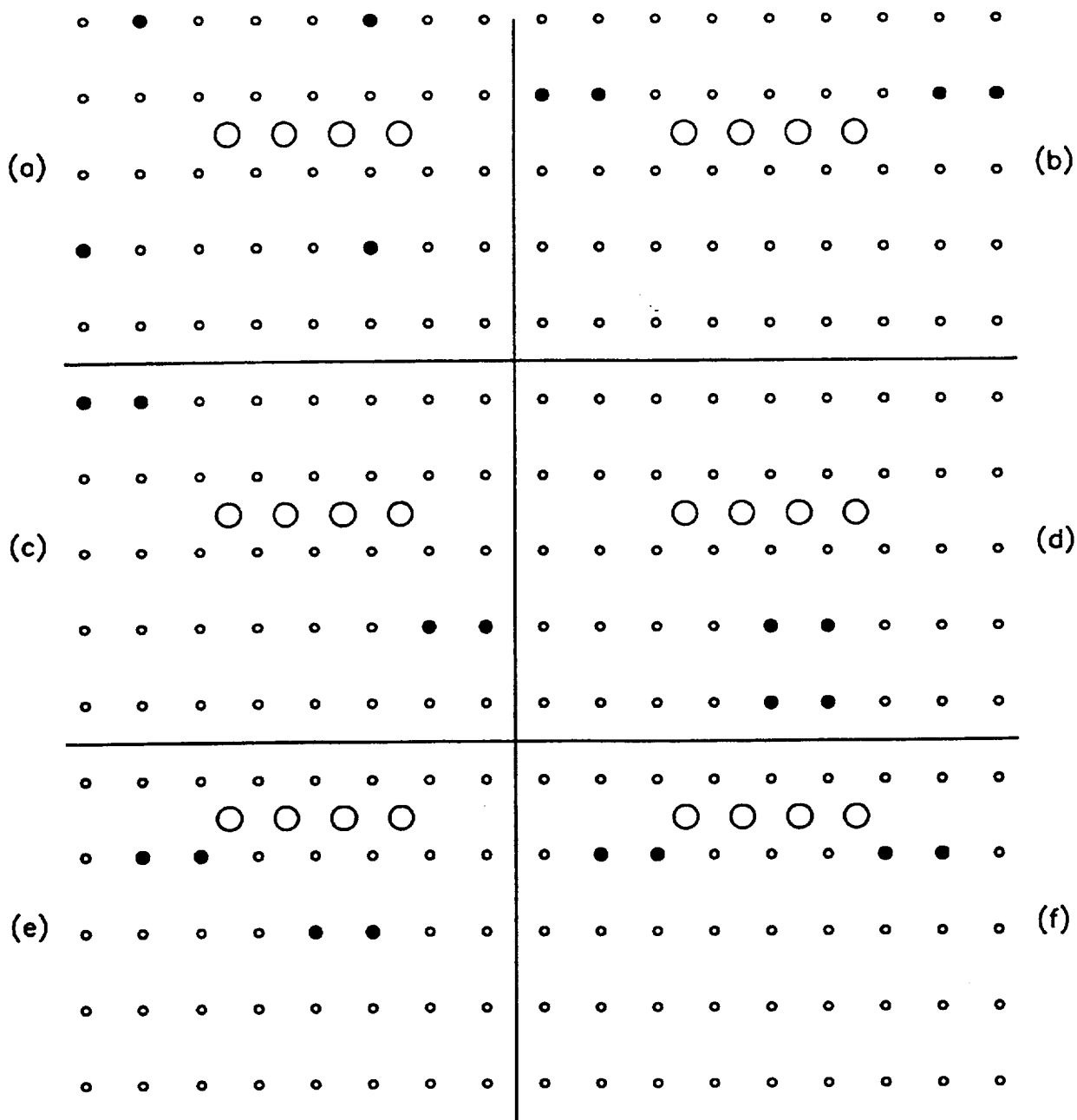


Fig. 2 : Schematic representation of the Ni(110) surface: as in fig. 1, small circles (o indicate Ni atoms in the surface layer; large circles (O) indicate Ni atoms displaced to the overlayer; Au atoms are indicated by large disks (●) when in the overlayer and with small disks (•) when occupying Ni sites in the surface plane. These configurations also correspond to a Au coverage of 0.067 ML.

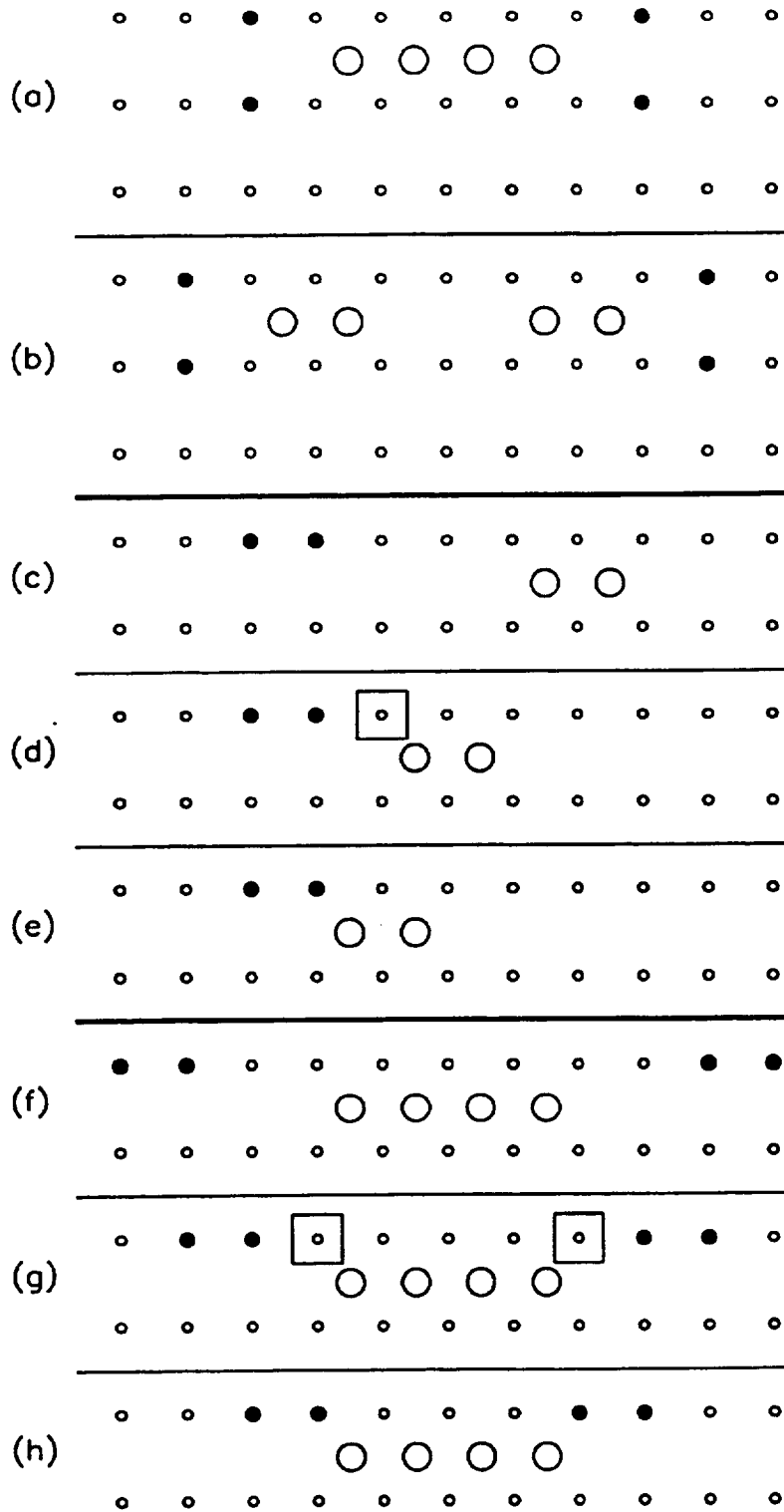


Fig. 3 : Using the convention indicated in fig. 2, the configurations shown correspond to a Au coverage of 0.067 ML.

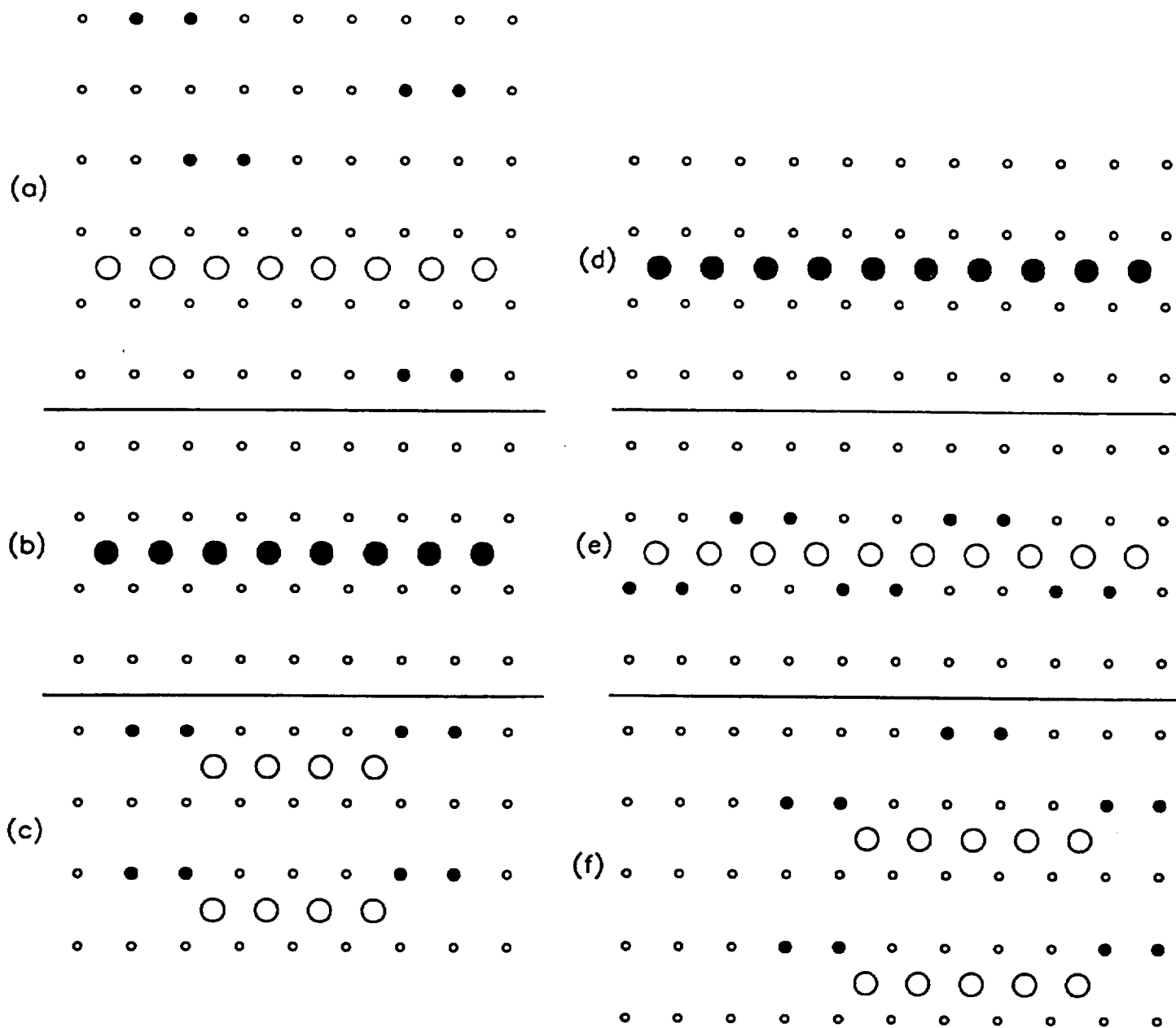


Fig. 4 : Using the convention indicated in fig. 2, the configurations shown correspond to a Au coverage of 0.13 ML (for (a),(b) and (c)) and 0.17 ML (for (d), (e) and (f)).

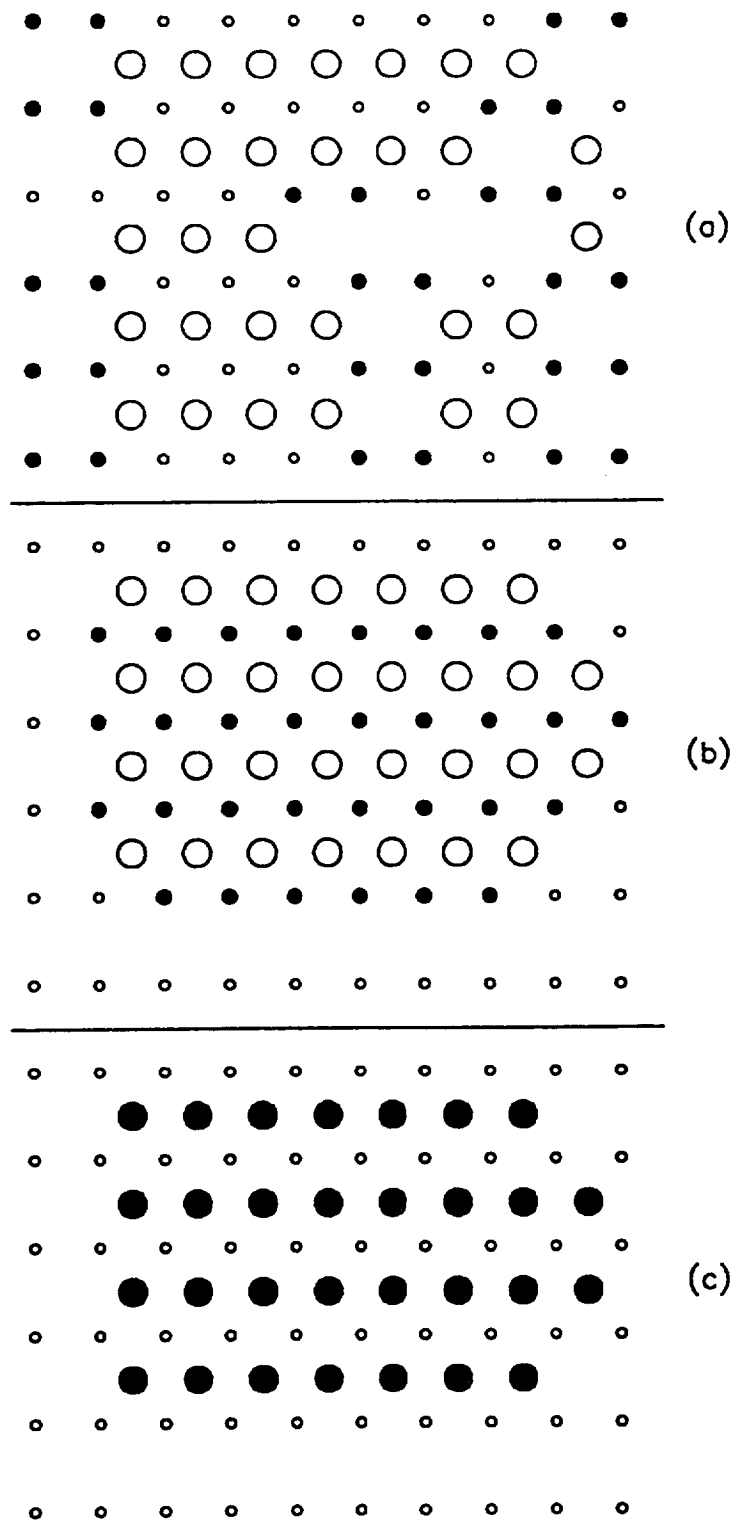


Fig. 5: Using the convention indicated in fig. 2, the configurations shown correspond to a Au coverage of 0.50 ML.

REPORT DOCUMENTATION PAGEForm Approved
OMB No. 0704-0188

Public reporting burden for this collection of information is estimated to average 1 hour per response, including the time for reviewing instructions, searching existing data sources, gathering and maintaining the data needed, and completing and reviewing the collection of information. Send comments regarding this burden estimate or any other aspect of this collection of information, including suggestions for reducing this burden, to Washington Headquarters Services, Directorate for Information Operations and Reports, 1215 Jefferson Davis Highway, Suite 1204, Arlington, VA 22202-4302, and to the Office of Management and Budget, Paperwork Reduction Project (0704-0188), Washington, DC 20503.

1. AGENCY USE ONLY (Leave blank)		2. REPORT DATE September 1994	3. REPORT TYPE AND DATES COVERED Technical Memorandum	
4. TITLE AND SUBTITLE Growth of Au on Ni(110): A BFS Modelling of Surface Alloy Phases			5. FUNDING NUMBERS WU-505-90-53	
6. AUTHOR(S) Guillermo Bozzolo, Rodrigo Ibañez-Meier, and John Ferrante				
7. PERFORMING ORGANIZATION NAME(S) AND ADDRESS(ES) National Aeronautics and Space Administration Lewis Research Center Cleveland, Ohio 44135-3191			8. PERFORMING ORGANIZATION REPORT NUMBER E-9108	
9. SPONSORING/MONITORING AGENCY NAME(S) AND ADDRESS(ES) National Aeronautics and Space Administration Washington, D.C. 20546-0001			10. SPONSORING/MONITORING AGENCY REPORT NUMBER NASA TM-106732	
11. SUPPLEMENTARY NOTES Guillermo Bozzolo, Analex Corporation, 3001 Aerospace Parkway, Brook Park, Ohio 44142 (work funded by NASA Contract NAS3-25776); Rodrigo Ibañez-Meier, WSA, Inc., 555 Bryant Street Palo Alto, California 94301; John Ferrante, NASA Lewis Research Center. Responsible person, John Ferrante, organization code 0130, (216) 433-6069.				
12a. DISTRIBUTION/AVAILABILITY STATEMENT Unclassified - Unlimited Subject Category 26			12b. DISTRIBUTION CODE	
13. ABSTRACT (Maximum 200 words) Recent experiments using scanning tunneling microscopy show evidence for the formation of surface alloys of otherwise immiscible metals. Such is the case for Au deposited in Ni(110), where experiments by Pleth Nielsen et al. indicate that at low Au coverage (<0.5 ML), Au atoms replace Ni atoms in the surface layer forming a surface alloy while the Ni atoms form islands on the surface. In this work, we present results of a theoretical modelling of this phenomenon using the recently developed BFS method for alloys. We provide results of an extensive analysis of the growth process which strongly support the conclusions drawn from the experiment: at very low coverages, there is a tendency for dimer formation on the overlayer, which later exchange positions with Ni atoms in the surface layer, thus accounting for the large number of substituted dimers. Ni islands formation as well as other alternative short range order patterns are discussed.				
14. SUBJECT TERMS Alloys; Surfaces			15. NUMBER OF PAGES 27	
			16. PRICE CODE A03	
17. SECURITY CLASSIFICATION OF REPORT Unclassified	18. SECURITY CLASSIFICATION OF THIS PAGE Unclassified	19. SECURITY CLASSIFICATION OF ABSTRACT Unclassified	20. LIMITATION OF ABSTRACT	